

A theoretical study of structure and stability of borohydride on 3d transition metals

メタデータ	言語: English 出版者: 公開日: 2015-03-18 キーワード (Ja): キーワード (En): 作成者: Arevalo, Ryan Lacdao, Escano, Mary Clare Sison, Gyenge, Elod, Kasai, Hideaki メールアドレス: 所属:
URL	http://hdl.handle.net/10098/8733

A theoretical study of the structure and stability of borohydride on 3d transition metals

Ryan Lacdao Arevalo^{1,a)}, Mary Clare Sison Escaño¹, Elod Gyenge²
and Hideaki Kasai^{1,b)}

¹Department of Precision Science & Technology and Applied Physics, Osaka University,

2-1 Yamadaoka, Suita, Osaka 565-0871, Japan

²Department of Chemical and Biological Engineering, The University of British

Columbia, Vancouver, BC V6T 1Z3, Canada

a) on leave from: Department of Physical Sciences, Philippine Normal University,
Manila 1000, Philippines

b) Corresponding Author: kasai@dyn.ap.eng.osaka-u.ac.jp

Abstract

The adsorption of borohydride on 3d transition metals (Cr, Mn, Fe, Co, Ni and Cu) was studied using first principles calculations within spin-polarized density functional theory. Magnetic effect on the stability of borohydride is noted. Molecular adsorption is favorable on Co, Ni and Cu, which is characterized by the strong $s-d_{zz}$ hybridization of the adsorbate-substrate states. Dissociated adsorption structure yielding one or two H adatom fragments on the surface is observed for Cr, Mn and Fe.

Keywords:

Density functional theory, Borohydride, 3d transitional metals, magnetic effect.

Introduction

Understanding the structure, energetics, and mechanism of adsorption of borohydride ($\text{BH}_{4\text{ads}}$) (“ads” means adsorbed on the surface) on different metals is an important step in the design and engineering on the atomic scale of surface catalysts for reactions involving borohydride. This is essential, for example, to guide the choice of anode catalyst for Direct Borohydride Fuel Cell (DBFC).

DBFC is an alkaline-based fuel cell which has a potential to generate high power densities competitive to Direct Methanol Fuel Cell (DMFC) for portable power applications [1]. Over an electrocatalyst selective to direct oxidation, each borohydride molecule is capable of producing eight electrons via the suggested over-all cell reaction:

$$\text{. (1)}$$

However, the efficiency and power density of DBFCs are limited in part by the lack of an effective anode electrocatalyst [2-4] and the competing non-selective hydrolysis reaction which leads to undesirable hydrogen gas evolution [5-8].

Many experimental studies on the electrooxidation of borohydride were carried out since the initial introduction of an aqueous sodium borohydride solution as an anode fuel for alkaline fuel cell in the 1960's [9-12]. Low coulombic efficiency was reported

for Ni, Pd, and Pt [5,7] due to the production of hydrogen gas. Au [13-14] and Ag [14] anodes were reported to have high coulombic efficiency but the slow electrode kinetics requires high overpotentials to attain a practical power density. Other electrochemical studies involved pure and alloy catalysts using a variety of experimental techniques [15-24]. The general picture that emerged from these studies is that the initial adsorption of borohydride anion (BH_y^-) on catalysts, accompanied by a simultaneous transfer of electron generating BH_{y-1} (with $y=1,2,3$ for dissociative and $y=4$ for molecular adsorption), and followed by electrocatalytic reactions of BH_{yads} with H_2O , OH_{ads} , and OH^- can explain, in principle, the electrooxidation process²⁵.

Despite the large number of experimental studies, only a few theoretical studies were made on the adsorption of borohydride on different metals [25-29]. For the case of Pt(111), Pd(111) and Ir(111) surfaces, we previously found that borohydride dissociates generating BH_{ads} and 3H_{ads} fragments [25]. The dissociated geometries differ only in the most stable sites for H_{ads} (i.e, Pd: fcc hollow site, Ir: top site, Pt: next-neighboring top site). These are the same sites that were proposed as the preferred locations for H adatoms on Pd, Ir and Pt in the absence of borohydride species [30-31]. Surface diffusion of H_{ads} and associative desorption yielding H_2 is very likely. This explains the experimental observation of high H_2 evolution on Pt [5,17]. Thus, a possible way to

avoid hydrogen evolution is to promote the molecular adsorption of borohydride on the metal surface. This molecularly adsorbed state was found for Au [25,27], Os, Ag, Rh, and Ru [25] surfaces (no $\text{H}_2\text{O}_{\text{ads}}$ coadsorption). Low adsorption energy for the case of Au causes the experimentally reported low surface coverage by adsorbed species. Thus, high overpotentials are required to achieve an appreciable rate of oxidation on Au [14]. A desired anode catalyst for direct oxidation, must therefore promote a strong molecular adsorption of borohydride to produce high surface coverage by reactive species [29] and avoid hydrogen evolution.

In this paper, we study the adsorption of borohydride on 3d transition metals (Cr, Mn, Fe, Co, Ni, and Cu) using first principles calculations within density functional theory (DFT). These metals are usually employed as alloying materials for various catalytic surfaces for fuel cell applications [32-41]. An understanding on how borohydride interacts with these alloying components can aid in the design of metal alloys or overlayers that are often considered experimentally. We present the adsorption energy of borohydride on these metals and then show the effect of the magnetic properties of the metals on the stability of borohydride on the surface. Then, we describe electronically the possible structures of borohydride on the surface and show that unique structures on 3d transition metals, different from those on noble metals, can

be achieved. To the best of our knowledge, the available literature still lacks a thorough fundamental understanding of the interaction of borohydride on the 3d metal surfaces considered in the present work.

Computational Model

The Cr, Mn, Fe, Co, Ni, and Cu (111) surfaces were modeled using a four-layer slab in a (3×3) unit cell making $\sim 1/9$ ML of adsorbate coverage. The fcc (111) facet of these metals was used to rule out the structural differences between different surfaces and to extract meaningful trends in properties as a function of substrate identity. This is certainly realistic for Ni and Cu since they occur naturally as fcc metals. For Cr, Mn, Co, and Fe, these fcc phases are important when considering epitaxial growth on substrates such as copper [42]. The calculated lattice constants for Cr, Mn, Fe, Co, Ni, and Cu are respectively: 3.61Å, 3.50Å, 3.45Å, 3.45Å, 3.53Å, and 3.68Å, in excellent agreement with those reported in the literatures (Cr: 3.62Å [43], Mn: 3.30Å to 3.57Å [44], Fe: 3.60Å [45], Co: 3.31Å to 3.51Å [44], Ni: 3.52Å [46], Cu: 3.61Å [47]). Each slab is separated by ~ 15.0 Å of vacuum, which is large enough to avoid the surface atom interaction along z axis with the neighboring unit cells. Electric dipole correction layer

in the vacuum area was used to cut the dipole interactions between the repeated image layer systems. Optimization is terminated when the Hellman-Feynman forces acting on each atom dropped below $0.005\text{eV}/\text{\AA}$.

The adsorption of borohydride anion (BH_4^-) has been experimentally discussed on both noble and non-noble metal catalysts [13,15,20-24,48-49] and found to be accompanied by a simultaneous transfer of electron to the electrode:



The adsorption of borohydride on metal surfaces can be modeled in an overall neutral unit cell. This model was also utilized in other related DFT studies on borohydride [25-29] and for oxidative adsorption of other anions like CO_3^{2-} [50] and OH^- [51-52].

The most stable configuration of adsorbed borohydride ($\text{BH}_{4\text{ads}}$) was determined by exhausting the possible orientations on the metal surface. This includes the H-up and H-down orientations (Fig. 1) of the tetragonal borohydride with B at the high symmetry sites on the surface (top, bridge, hcp hollow and fcc hollow sites) and in-plane rotation. The adsorbate and the top two layers of the slab were fully relaxed in all directions while the bottom two layers of the slab were held fixed at their bulk structure. The adsorption energy, E_{ads} , on each metal was computed by taking the difference between the total energy of the borohydride-slab system in the lowest energy

adsorption site and the summed energies of the relaxed clean surface and gas-phase borohydride.

Spin polarized density functional theory (DFT) calculations were implemented via the Vienna ab initio simulation package (VASP) [53-56]. The interaction between ions and electrons were described using projector augmented wave (PAW) method [57-58]. Plane wave basis sets were employed with energy cut-off of 400eV. The exchange-correlation term was described using generalized gradient approximation (GGA) based on Perdew-Burke-Ernzerhof (PBE) [59-60] functional. The surface Brillouin zone integrations were performed on a grid of (4×4×1) Monkhorst-Pack k-points [61] using Methfessel-Paxton smearing [62] of $\sigma = 0.2\text{eV}$. Conjugate-gradient algorithm [63] was used to relax the ions into their ground state. Convergence of numerical results with respect to the slab thickness, the kinetic energy cut-off and the k-point was established.

Results and Discussion

A. Stability and magnetic properties

Fig. 2 shows the calculated adsorption energies of tetrahedral borohydride on the (111) surfaces of the metals considered. We note that the adsorption energy generally decreases as we traverse the periodic table from left to right (Cr to Cu). Borohydride adsorption energy is strongest for Cr, followed by Fe, Mn, Co, Ni, and Cu, in decreasing order of magnitude (Fig. 2). The almost monotonic tendency of adsorption energies to decrease from Cr to Cu can be explained by the interaction of sp band of the adsorbate with the metal d band which results to the formation of bonding and antibonding states with respect to adsorption. The overall energetics depends on the extent of filling of the antibonding state with respect to the Fermi energy. This derived sp-d antibonding state follows the position of the metal d band. Moving from Cr to Cu, the d band moves further below the Fermi energy. Thus, the extent of filling of the antibonding state from Cr to Cu increases which contributes to a repulsive interaction.

Interestingly, Fe has a higher adsorption energy than the expected value from the trend of decreasing adsorption energies from Cr to Cu (as shown by the red data

point in Fig. 2). This can be explained by the magnetic properties of Fe. For all these metals (except for Cu which has a non-spin-polarized d band), the adsorption of borohydride results in the change of the d-band fractional occupancy, n_d projected on the surface metal atom. Here, n_d is defined as:

$$\frac{\int_{E_F}^{E_d} \rho_d(E) dE}{\int_{E_d} \rho_d(E) dE} \quad (3)$$

where E_F is the Fermi level and ρ_d is the d band density of states. Note that the numerator and denominator were evaluated within the occupied states and whole d-band, respectively.

The reduction of the spin-up and the increase of the spin-down d-band fractional occupancy, respectively, causes the forward shifting of the spin-up and backward shifting of the spin-down components of the d-band before and after adsorption as shown schematically in Fig. 3. This phenomenon is accompanied by the change of the total magnetic moment for the three metal atoms directly bonded to borohydride. A dramatic change in the magnitude of the magnetic moment is seen for Fe ($3.78\mu_B$), compared to relatively small changes for the other metals (Cr: $0.942\mu_B$, Mn: $0.632\mu_B$, Co: $0.924\mu_B$, Ni: $0.588\mu_B$). A similar demagnetization of the substrate upon the adsorption of molecules was reported in several works [64-66]. This finding is supported by the largest change in the spin-up and spin-down d-band fractional

occupancy, Δn_d , of Fe compared to other metals before and after the adsorption (Table I). Thus, the large asymmetric shift of the Fe d-band has a stabilizing effect on the adsorption of borohydride. The changes in the d-band fractional occupancy are reported in Table I.

A comparison of the calculated adsorption energies for these metals with 4d and 5d transition metals is shown in Fig. 4. The adsorption energy for Cr, Mn and Fe (-7.14eV, -4.93eV and -5.36eV, respectively) are much greater than the reported strong adsorption on other transition metals (Pt: -4.40eV, Ir: -4.40eV, Os: -4.43eV, and Ru: -4.22eV) [25], computed using the same parameters such as adsorbate coverage and number of slab layers. The lower adsorption energy (-4.09eV) previously reported [26] for 0.25ML coverage of borohydride on Mn(111) implies the enhanced repulsive interaction between adsorbates as coverage is increased. The small adsorption energy for Cu (-2.87eV) can be explained by the full occupancy of its d-orbitals. This relatively small adsorption energy was also observed previously for the case of other metals with fully occupied d band (Ag: -1.98eV, Au: -1.69eV) [25]. The trend of decreasing magnitude of adsorption energy (from Cu, Ag to Au) was also observed in other DFT studies [67-70]. To explain this trend, note that the other factor that affects the adsorption energy is the repulsive energy cost of orthogonalization between borohydride

sp and metal d states as dictated by Pauli exclusion principle. This orthogonalization energy increases as the d orbital becomes more extended. Moving from Cu, Ag to Au, the d orbital becomes more extended making the adsorption energy decrease from Cu, Ag to Au.

B. Molecular adsorption

For Co, Ni and Cu surfaces, borohydride molecularly chemisorbs through the H-up orientation with boron above the fcc hollow site and hydrogen atoms residing at the top sites (Fig. 5a). Here, molecular adsorption is categorized based on the B-H bond length (Fig. 4): between 1.26Å (gas-phase bond length) and 1.49Å (elongated bond length).

For the other metals considered in this study (Mn, Fe and Cr), stable molecular adsorption structure was also found but at lower adsorption energy (more weakly bound) compared to the dissociated structure, which we will discuss in the next section. The preference for the fcc hollow over the hcp hollow site is very small ($\sim 0.02\text{eV}$). This means that the presence (or absence) of atoms just below the hcp (or fcc) hollow site does not significantly affect the adsorption energetics. This supports the previous

findings wherein a small preference between the fcc and hcp hollow sites were found for 4d and 5d transition metals [25,27-28]. The distances from the surface hydrogen atom to the nearest metal atom are 1.63Å, 1.60Å, and 1.70Å on Co, Ni, and Cu, respectively. The bond length between boron and hydrogen atoms near the metal surface has increased from 1.25Å in the gas phase to 1.33Å, 1.33Å, and 1.26Å on Co, Ni, and Cu, respectively. The H-B-H angles are 91.7°, 90.2° and 96.5° for Co, Ni, and Cu respectively. Based on the previously reported results [25], borohydride has the same B-H bond length on Cu and Au. For Co and Ni, the B-H bond lengths fall within the reported molecular adsorption structure of borohydride on other transition metals (1.26-1.49Å) [25]. For comparison, the B-H bond lengths of borohydride on other metals were shown in Fig. 4.

To understand the electronic factors that determine the bonding of borohydride on these surfaces, we analyzed the density of states (DOS) of the system. For the molecular adsorption at the hollow site, the broadening and shifting of DOS is prominent only on the d_{zz} state while the other states are essentially unchanged. In Fig. 6, we show this state for the case of Cu as a representative metal. There is a formation of new peaks below the bottom of the d_{zz} -projected DOS of the metals, which resonate with the surface H-s orbitals of borohydride. This forms the bonding state between the

metal and borohydride. Thus, the molecular adsorption of borohydride at the hollow site is characterized by the strong hybridization of metal- d_{zz} state with H-s state. This is illustrated by the partial charge density distribution projected using 0.01 electron/ a_0^3 isosurface value at an identified bonding state shown in the inset of Fig. 6. Here, the mixing between charge density of the H atoms and the metal is very evident. This hybridization is promoted when borohydride is in H-up orientation, which explains its stability over the H-down orientation.

C. Dissociative adsorption

For the case of Mn and Fe surfaces, the adsorption at the bridge site (i.e., B on top of the bridge site) produces $BH_{2ads} + 2H_{ads}$ species as shown in Fig. 5b. This configuration is 0.11eV and 0.02eV lower in energy than the molecular adsorption of borohydride at the hollow site of Mn and Fe, respectively. This structure was not found to be stable neither on the 4d and 5d metals previously studied [25] nor on the other metals presented in this paper. The dissociated hydrogen atoms (H1 and H2 in Fig. 5b) reside on the neighboring hollow sites. BH_{2ads} forms a bent structure on the plane perpendicular to the surface with inner angle equal to 102° for both Mn and Fe. The

B-H1 and B-H2 distances are reported in Table I. Thus, there exists a BH_4 chemisorption situation where 2H_{ads} are formed rather than the more commonly reported 3H_{ads} case, which was previously found for Ir, Pd, and Pt [25].

For the 2H_{ads} configuration, our previous work [26] has revealed the importance of d_{zz} state of the atom M1 and $d_{xz,yz}$ states of atom M2 (indexed in Fig. 5b). The competing d_{zz} and $d_{xz,yz}$ interactions of the metal aimed at H and B of borohydride results in an enhanced elongation of the two B-H bonds (B-H1 and B-H2 in Fig. 5b). The B-H bond lengths of borohydride adsorbed at the bridge site of these surfaces is reported in Table I for reference.

It may be interesting to infer why this 2H_{ads} dissociated configuration is attainable at the bridge site of Mn and Fe but not on other metals. Because of the very strong adsorption of borohydride on these metals compared to all other metals considered in this paper and previous literature [25-26], borohydride gets much closer to Mn and Fe surfaces (Mn: 1.42Å and Fe: 1.41Å) compared to other metals (Co: 1.59Å, Ni: 1.54Å, and Cu: 1.86Å). This leads to a stronger competition of the d_{zz} and $d_{xz,yz}$ states described earlier, which causes a greater B-H1 and B-H2 bond elongation. As shown in Table I, the B-H1 and B-H2 bond lengths increase as the distance of boron from the surface (z) decreases. Thus, because of the very strong adsorption of

borohydride on Mn and Fe metals, different adsorption structures of borohydride may be observed on the different sites of the same metal (i.e., molecular on hollow site or dissociated at bridge site).

Furthermore, a unique dissociated adsorption configuration was found for the case of the Cr surface. The adsorption of borohydride generates the dissociation of one B-H bond yielding $\text{BH}_{3\text{ads}} + \text{H}_{\text{ads}}$ fragments on the surface. As shown in Fig. 5c, the dissociated H atom is at 2.28Å distance from B while the B-H bond lengths for $\text{BH}_{3\text{ads}}$ are within 1.20-1.33Å. This structure is 0.16eV lower in energy than the molecularly adsorbed borohydride on the hollow site (just like in Fig. 5a). We note a complex lateral relaxation of the top two layers of the Cr slab to accommodate this dissociated structure of borohydride. Such large distortion on the surface makes it difficult to analyze the adsorption structure electronically. The other metals that yield the dissociated structure for borohydride are shown in Fig. 4.

These results pose relevant insights in the use of the metals considered in this paper as alloying components in the design of anode catalyst for DBFC. As discussed in the Introduction, high coulombic efficiency of borohydride oxidation can be achieved on Au but at high overpotential. To enable the oxidation activity at lower potential, it is reasonable to alloy Au with 3d transition metals which can promote stronger adsorption

interaction than pure Au and at the same time retain its molecular structure as on Au. Our preliminary results of such systems have shown that molecular adsorption structure with greater adsorption energy compared to pure Au can be achieved on these Au-based alloys. Recently, Au-3d metal alloys were experimentally shown to be inactive to hydrogen evolution and require lower overpotential compared to pure Au [71-73]. Detailed discussion of such systems will be published elsewhere.

Conclusion

The structure and stability of borohydride on 3d transition metals (Cr, Mn, Fe, Co, Ni and Cu) was studied using first principles calculations within spin-polarized density functional theory. The adsorption energy was highest on Cr, followed by Fe, Mn, Co, Ni and Cu, in decreasing order of magnitude. Magnetic effect on the stability of borohydride is noted. The forward shifting of the spin-up and conversely the backward shifting of the spin-down components of the d-band, before and after the adsorption of borohydride, was most pronounced for the case of Fe substrate. This had a stabilizing effect on the adsorption of borohydride. Molecular adsorption was favorable on Co, Ni and Cu, which is characterized by strong s-d_{zz} hybridization of the adsorbate-substrate

states. Dissociated adsorption structures yielding one or two H adatom fragments on the surface, was observed for Cr (generating $\text{BH}_{3,\text{ads}} + \text{H}_{\text{ads}}$), and Mn, Fe (generating $\text{BH}_{2,\text{ads}} + 2\text{H}_{\text{ads}}$). These results pose relevant insights in the use of these alloying metals in the design of anode catalysts for direct borohydride fuel cell.

Acknowledgement

This work is supported in part by MEXT (Ministry of Education, Culture, Sports, Science and Technology) through the G-COE (Special Coordination Funds for the Global Center of Excellence) program "Atomically Controlled Fabrication Technology", Grant-in-Aid for Scientific Research on Innovative Areas Program (2203-22104008) and Scientific Research (c)(22510107) program, and JST (Japan Science and Technology Agency) through ALCA (Advanced Low Carbon Technology Research and Development) Program. Some of the calculations were done using the computer facilities of Cyber Media Center (Osaka University), ISSP Super Computer Center (University of Tokyo), and Large Scale Simulation Program KEK No.T10-12 of High Energy Accelerator Research Organization. R.L. Arevalo acknowledges the Ministry of Education, Culture, Sports, Science and Technology (MEXT) for

scholarship grant. M.C. Escaño extends her gratitude to Japan Society for Promotion of Science (JSPS) Fellowship for research funds.

References

- [1] J.-H. Wee, *J. Power Sources* 161 (2006) 1.
- [2] Z.P. Li, B.H. Liu, K. Arai and S. Suda, *J. Alloy Compd.* 404 (2005) 648.
- [3] C.P. de Leon, F.C. Walsh, D. Pletcher, D.J. Browning and J.B. Lakeman, *J. Power Sources* 155 (2006) 172.
- [4] J.-H. Wee, *J. Power Sources* 155 (2006) 329.
- [5] E. Gyenge, *Electrochim. Acta* 49 (2004) 965.
- [6] J.I. Martins, M.C. Nunes, R. Koch, L. Martins and M. Bazzaoui, *Electrochim. Acta* 52 (2007) 6443.
- [7] B.H. Liu, Z.P. Li and S. Suda, *Electrochim. Acta* 49 (2004) 3097.
- [8] B.H. Liu, Z.P. Li and S. Suda, *J. Electrochem. Soc.* 150 (2003) A398.
- [9] J.P. Elder, *Electrochim. Acta* 7 (1962) 417.
- [10] J.P. Elder and A. Hickling, *Trans. Faraday Soc.* 58 (1962) 1852.
- [11] M.E. Indig and R.N. Snyder, *J. Electrochem. Soc.* 109 (1962) 1104.
- [12] H. Brown and C.A. Brown, *J. Am. Chem. Soc.* 84 (1962) 1493.
- [13] V. Mirkin, H. Yang and A.J. Bard, *J. Electrochem. Soc.* 139 (1992) 2212.
- [14] M. Chatenet, F. Micoud, I. Roche and E. Chainet, *Electrochim. Acta* 51 (2006) 5459.
- [15] E. Gyenge, M. Atwan and D. Northwood, *J. Electrochem. Soc.* 153 (2006) A150.

- [16] V. Lam and E. Gyenge, *J. Electrochem. Soc.* 155 (2008) B1155.
- [17] V. Lam, D. Kannangara, A. Alfantazi and E. Gyenge, *J. Phys. Chem. C* 115 (2011) 2727.
- [18] D. Finkelstein, N. Da Mota, J. Cohen and H. Abruna, *J. Phys. Chem. C* 113 (2009) 19700.
- [19] H. Cheng and K. Scott, *Electrochim. Acta* 51 (2006) 3429.
- [20] B. Molina Concha and M. Chatenet, *Electrochim. Acta* 54 (2009) 6119.
- [21] B. Molina Concha, M. Chatenet, E. Ticianelli and F. Lima, *J. Phys. Chem. C* 115 (2011) 12439.
- [22] M. Simoes, S. Baranton and C. Coutanceau, *Electrochim. Acta* 56 (2010) 580.
- [23] M. Simoes, S. Baranton and C. Coutanceau, *J. Phys. Chem. C* 113 (2009) 13369.
- [24] V. Kiran, T. Ravikumar, N. Kalyanasundaram, S. Khrishnamurty, A. Shukla and S. Sampath, *J. Electrochem. Soc.* 157 (2010) B1201.
- [25] M.C.S. Escano, E. Gyenge, R.L. Arevalo and H. Kasai, *J. Phys. Chem. C* 115 (2011) 19883.
- [26] R.L. Arevalo, M.C.S. Escano and H. Kasai, *e-J. Surf. Sci. Nanotech.* 9 (2011) 257.
- [27] G. Rostamikia and M.J. Janik, *J. Electrochem. Soc.* 156 (2009) B86.
- [28] G. Rostamikia and M.J. Janik, *Electrochim. Acta* 55 (2010) 1175.
- [29] G. Rostamikia and M.J. Janik, *Energy and Envi. Sci.* 3 (2010) 1262.
- [30] N. Ozawa, T.A. Roman, H. Nakanishi, H. Kasai, N.B. Arboleda, W.A. Dino, *J. Appl. Phys.* 101 (2007) 123530.
- [31] S.C. Badescu, P. Salo, S.C. Ying, K. Jacobi, Y. Wang, K. Bedurftig, G. Ertl,

- Phys. Rev. Lett. 246 (2002) 136101.
- [32] A.A.B. Padama, M.C.S. Escano, M.Y. David, H. Kasai and H. Kawai, *e-J. Surf. Sci. Nanotech.* 8 (2010) 325.
- [33] H. Dipojono, A. Saputro, S. Aspera and H. Kasai, *Jpn. J. Appl. Phys.* 50 (2011) 055702.
- [34] M.C. Escano, E. Gyenge, H. Nakanishi and H. Kasai, *J. Nanosci. Nanotechnol.* 11 (2011) 2944.
- [35] M.C. Escano, H. Nakanishi and H. Kasai, *J. Phys. Chem. A* 113 (2009) 14302.
- [36] M. Escano, T. Nguyen, H. Nakanishi and H. Kasai, *Surf. Sci.* 602 (2008) 1.
- [37] M.C. Escano, H. Nakanishi and H. Kasai, *Surf. Interface Anal.* 40 (2008) 1085.
- [38] T. Brylewski, M. Nanko, T. Maruyama and K. Przybulski, *Solid State Ionics* 143 (2001) 2.
- [39] A. Shukla, R. Raman, N. Choudhury, K. Priolkar, P. Sarode, S. Emura and R. Kumashiro, *J. Electroanal. Chem.* 563 (2004) 181.
- [40] L. Xiong, A. Kannan and A. Manthiram, *Electrochem. Comm.* 4 (2002) 898.
- [41] K. Park, J. Choi, B. Kwon, S. Lee and Y. Sung, *J. Phys. Chem. B* 106 (2002) 1869.
- [42] J. Shen, Z. Gai and J. Kirschner, *Surf. Sci.* 52 (2004) 163.
- [43] H.H. Wang and G.Y. Guo, *J. Magn. Magn. Mater.* 209 (2000) 98.
- [44] M.J. Mehl and D.A. Papaconstantopoulos, *Phys. Rev. B* 54 (1996) 7.
- [45] M. Zhang, F. Pan and B.X. Liu, *J. Phys.: Condens. Matter* 9 (1997) 7623.
- [46] V. M. Schastlivtsev and V. V. Ustinov, *Doklady Akademii Nauk* 395 (2004) 3.
- [47] M. E. Straumanis and L. S. Yu, *Acta Cryst. A* 25 (1969) 676.
- [48] J.S. Zhang and W.N. Jiang, *J. Power Sources* 164 (2007) 772.

- [49] A.Y. Tsivadaze, M.R. Tarasevich, V.N. Titova, A.A. Yavich and N.V. Petrova, *Phys. Chem.* 414 (2007) 107.
- [50] Y. Kunisada, H. Kishi, F. Dimas, M. David, H. Nakanishi and H. Kasai, T. Asari, S. Hayashi, *Jpn. J. Appl. Phys.* 49 (2010) 02BB04.
- [51] H. Xin and S. Linic, *J. Chem. Phys.* 132 (2010) 221101.
- [52] J. Roques and A. Anderson, *J. Electrochem. Soc.* 151 (2004) E85.
- [53] G. Kresse and J. Furthmuller, *Comput. Mater. Sci.* 6 (1996) 15.
- [54] G. Kresse and J. Furthmuller, *Phys. Rev. B* 54 (1996) 11169.
- [55] G. Kresse and J. Hafner, *Phys. Rev. B* 47 (1993) 558.
- [56] G. Kresse and J. Hafner, *Phys. Rev. B* 49 (1994) 14251.
- [57] P.E. Blochl, *Phys. Rev. B* 50 (1994) 17953.
- [58] G. Kresse and J. Joubert, *Phys. Rev. B* 59 (1999) 1758.
- [59] J. Perdew, K. Burke and M. Ernzerhof, *Phys. Rev. Lett.* 77 (1996) 3865.
- [60] J. Perdew, K. Burke and M. Ernzerhof, *Phys. Rev. Lett.* 78 (1997) 1396.
- [61] H.J. Monkhorst and J.D. Pack, *Phys. Rev. B* 13 (1976) 5188.
- [62] M. Methfessel and A. Paxton, *Phys. Rev. B* 470 (1989) 3616.
- [63] I. Stich, R. Car, M. Parrinello and S. Baroni, *Phys. Rev. B* 39 (1989) 4997.
- [64] D. Spisak, J. Hafner, *Phys. Rev. B* 64 (2001) 094418.
- [65] J. Greeley, M. Mavrikakis, *J. Phys. Chem. B* 109 (2005) 3460.
- [66] G. Kresse, J. Hafner, *Surf. Sci.* 459 (2000) 287.
- [67] R.L. Arevalo and R.F. Pobre, *e-J. Surf. Sci. Nanotech.* 9 (2011) 251.
- [68] G. Wang, Y. Zhou and J. Nakamura, *J. Chem. Phys.* 122 (2005) 044707.
- [69] Y. Akinaga, T. Nakajima and K. Hirao, *J. Chem. Phys.* 114 (2001) 19.
- [70] J.R.B. Gomes and J.A.N.F. Gomes, *J. Mol. Struct.: Theochem.* 503 (2000) 189.

- [71] P. He, Y. Wang, X. Wang, F. Pei, H. Wang, L. Liu, L. Yi, *J. Power Sources*, 2011, 196, 1042.
- [72] P. He, X. Wang, Y. Liu, L. Yi, X. Liu, *Int. J. Hydrogen Energ.*, 2012, 37, 1254.
- [73] P. He, X. Wang, Y. Liu, L. Yi, *Int. J. Hydrogen Energ.*, 2012, in press.
- [74] G. Henkelman, B.P. Uberuaga, H. Johansson, *J. Chem. Phys.* 113 (2000) 9901.
- [75] G. Mills, H. Johansson, G.K. Schenter, *Surf. Sci.* 324 (1995) 305.

Table I: Change in the d-band fractional occupancy, Δn_d , B-H bond lengths and height z of boron from the surface to the bridge site on Cr, Mn, Fe, Co, Ni, and Cu.

Metal	Δn_d		z (Å)	B-H1 bond length (Å)	B-H2 bond length (Å)
	Spin up	Spin down			
Cr	-0.01	0.01	--*	--*	--*
Mn	-0.12	0.14	1.42	2.26	2.28
Fe	-0.26	0.27	1.41	2.19	2.18
Co	-0.04	0.03	1.59	1.49	1.46
Ni	-0.03	0.10	1.54	1.44	1.43
Cu	-0.01	-0.01	1.86	1.29	1.28

*Adsorption of borohydride at the bridge site of Cr surface results in a translation to the hollow site because of a negligible energy barrier. Compared to the case of Mn, the energy barrier for translation from the bridge to hollow site is 1.35eV, calculated using climbing image nudge elastic band method (CI-NEB) [74-75].

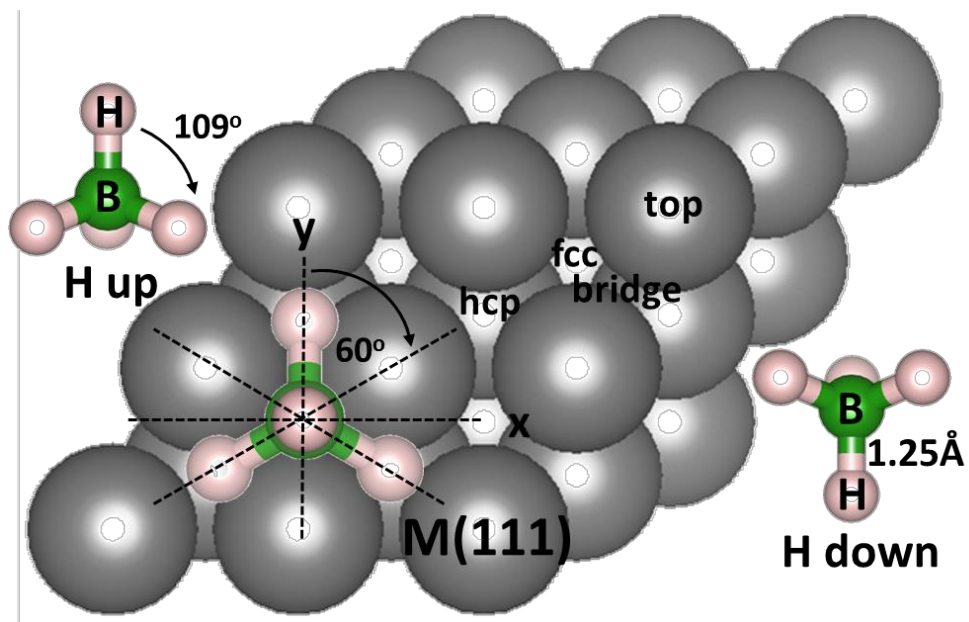


Fig. 1: The stable configuration of adsorbed borohydride ($\text{BH}_{4\text{ads}}$) was determined by initially placing the tetrahedral borohydride in H-up and H-down orientations with B at the high symmetry sites on the surface (top, bridge, hcp hollow and fcc hollow sites) and rotating the molecule on the xy plane.

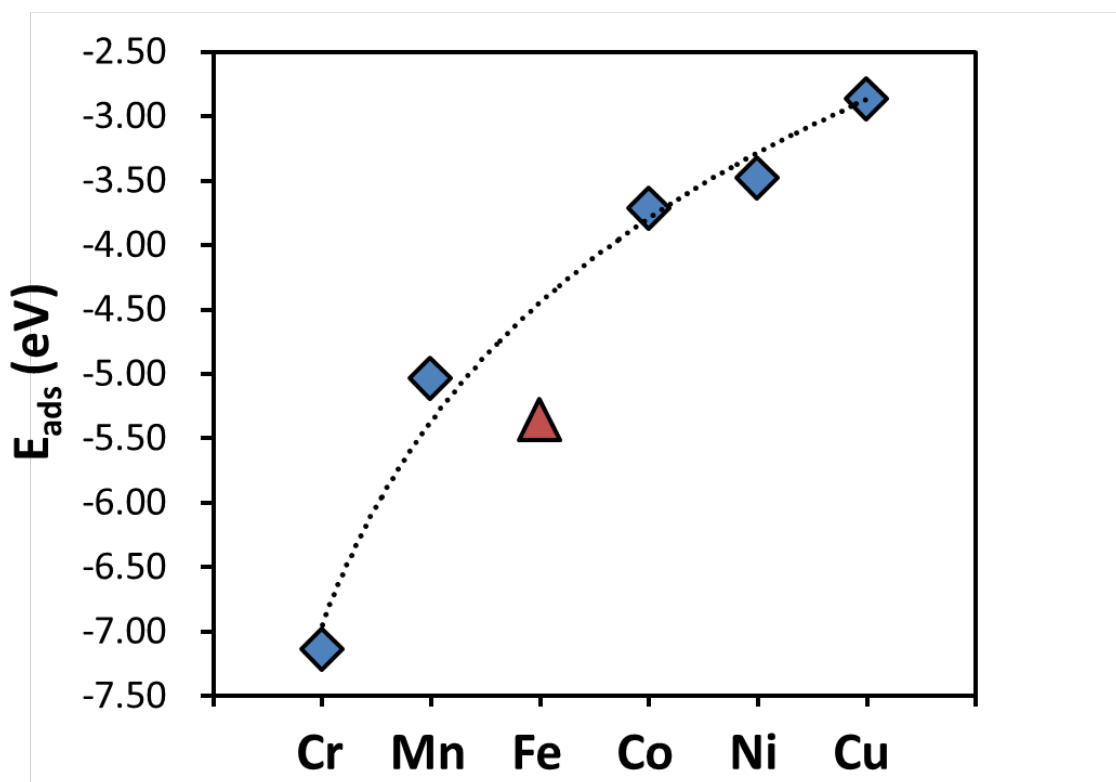


Fig. 2: The adsorption energy, E_{ads} of borohydride on Cr, Mn, Fe, Co, Ni, Cu. A trendline shown by the dashed curved was obtained by logarithmic curve fitting.

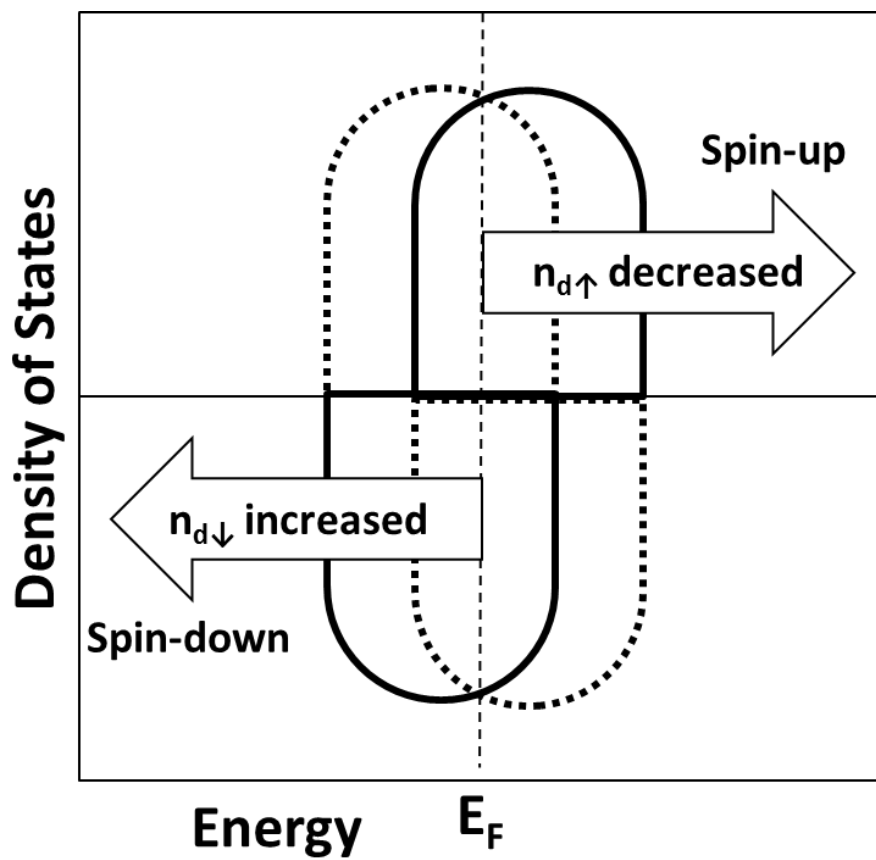


Fig. 3: A schematic diagram of the shifting of spin-up and spin-down components of the metal d-band before (dashed line) and after (solid line) the adsorption of borohydride.

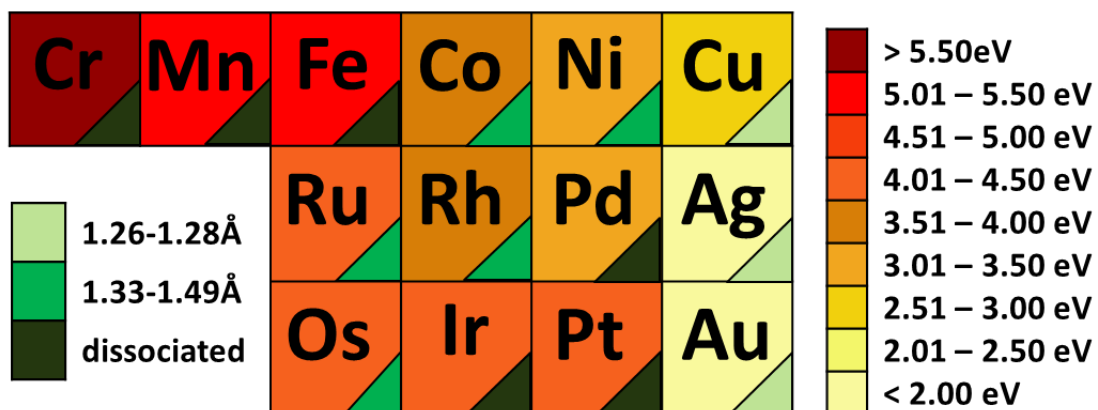


Fig. 4: A comparison of adsorption energies (in absolute values) and B-H bond lengths of borohydride on different metals.

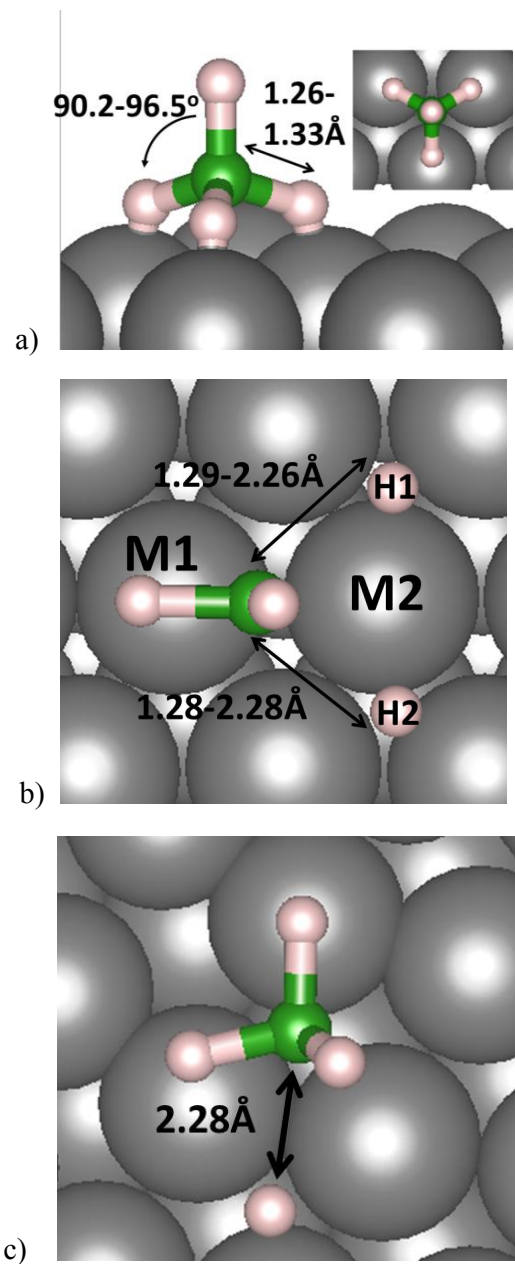


Fig. 5: The adsorption structure of borohydride: a) molecular adsorption for Co, Ni and Cu and dissociative adsorption for b) Mn and Fe; and c) Cr.

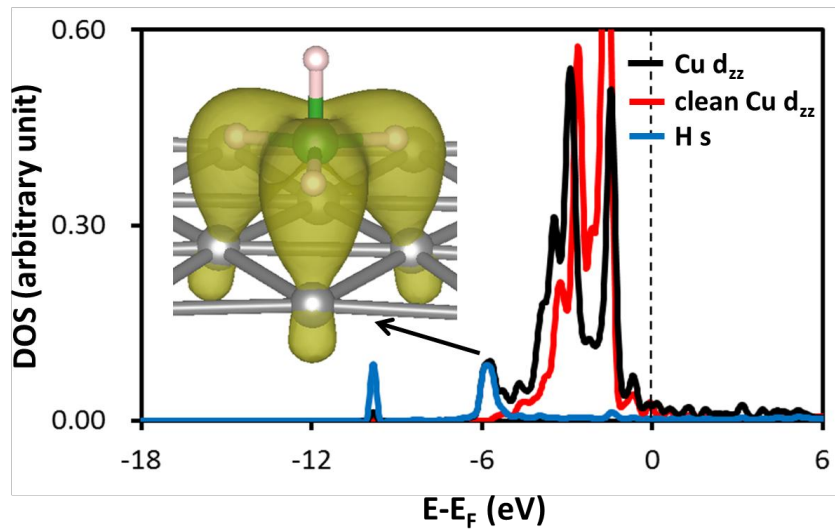


Fig. 6: Density of states projected on the d_{zz} state of the surface metal atom directly bonded to borohydride for Cu when borohydride is adsorbed at the hollow site. The red and black curves are for the clean and adsorbed states respectively. The inset figure shows the partial charge density distribution projected using 0.01 electron/ a_0 isosurface level on the bonding state shown by the arrow.

Figure Captions

Figure 1: The stable configuration of adsorbed borohydride ($\text{BH}_{4\text{ads}}$) was determined by initially placing the tetragonal borohydride in H-up and H-down orientations with B at the high symmetry sites on the surface (top, bridge, hcp hollow and fcc hollow sites) and rotating the molecule on the xy plane.

Figure 2: The adsorption energy, E_{ads} of borohydride on Cr, Mn, Fe, Co, Ni, Cu.

Figure 3: A schematic diagram of the shifting of the spin-up and spin-down components of the metal d-band before (dashed line) and after (solid line) the adsorption of borohydride.

Figure 4: A comparison of adsorption energies (in absolute values) and B-H bond lengths of borohydride on different metals.

Figure 5: The adsorption structure of borohydride: a) molecular adsorption for Co, Ni and Cu and dissociative adsorption for b) Mn and Fe; and c) Cr.

Figure 6: Density of states projected on the d_{zz} state of the surface metal atom directly bonded to borohydride for Cu when borohydride is adsorbed at the hollow site. The red and black curves are for the clean and adsorbed states respectively. The inset figure shows the partial charge density distribution projected using 0.01 electron/ a_0 isosurface level on the bonding state shown by the arrow.

Table Caption

Table I: Change in the d-band fractional occupancy, Δn_d , B-H bond lengths and height z of boron from the surface to the bridge site on Cr, Mn, Fe, Co, Ni, and Cu.